Influence of evaporation-condensation in reactive spreading.

Olivier Dezellus, F. Hodaj, Stefan Janaqi, N. Eustathopoulos

Influence of evaporation–condensation in reactive spreading

O. Dezellus [a], F. Hodaj [a], S. Janaqi [b], N. Eustathopoulos [a,*]

[a] *LTPCM-UMR 5614 CNRS-INPG-UJF/ENSEEG, BP 75, Domaine Universitaire, F-38402 Saint-Martin d'Hères Cedex, France*
[b] *Ecole des Mines d'Alès, site EERIE, LGI2M, Parc Scientifique Georges Besse, F-30035 Nîmes Cedex 1, France*

Abstract

In reactive wetting, considerable acceleration of spreading rate is usually observed in the high contact angle (short spreading time) range in comparison to the low contact angle range. This study examines the possibility to explain this acceleration by an evaporation–condensation process which may occur under high vacuum in front of the triple line. For this purpose, a method is developed to evaluate the thickness of the reaction product in front of the triple line during spreading. This method is based on calculations of ballistic exchange in vacuum between the drop and the substrate surfaces combined with Auger spectroscopic analysis of the substrate surface. The method is applied to Cu–40 at% Si and Cu–1.5 at% Cr droplets on vitreous carbon systems.

Keywords: Evaporation; Condensation; Wetting; Vacuum; Auger spectroscopy; Metals; Carbon

1. Introduction

Poor wetting is generally observed in non-reactive metal/oxide and metal/carbon systems. Indeed in these systems the angle θ formed at the contact line of three phases, solid, liquid and vapour, is often higher than 90° [1–3]. Typical examples are the couples Cu/Al_2O_3 and Cu/C, for which the contact angle under high vacuum is as high as 120–140°.

A considerable improvement in wetting can be produced in such systems using certain alloying elements which, by reaction with ceramic, form a continuous layer of wettable compound along the metal/ceramic interface. Such chemical reactions cause transitions in contact angle θ with time, measured during a sessile drop experiment, from an initial wetting angle θ_0 corresponding to the Young contact angle of the liquid on the original unreacted substrate surface, to a final stable value, θ_F, which nearly equals the Young contact angle of the liquid on the reaction product [4,5].

In view of the great interest presented in brazing of ceramics and electronic packaging, the dynamics of reactive wetting has been the subject of numerous studies published in recent years [6–13].

In non-reactive metal/metal or metal/ceramic systems, the time t_F for millimetre-sized molten droplets to reach capillary equilibrium is less than 0.1 s [3,14], which is much shorter than the spreading times observed in reactive systems (typically $10–10^4$ s). Starting from this observation, it was

* Corresponding author. Fax: +33-4-7682-6767.
E-mail address: nikos@ltpcm.inpg.fr (N. Eustathopoulos).

concluded in Ref. [7] that in reactive systems, the rate at which the droplet spreads is not limited by the viscous flow, but by the rate of the interfacial reaction itself.

The rate of the interfacial reaction, in turn, may be controlled by the slower of two successive phenomena that intervene in the reaction process: local reaction kinetics at the triple line, and diffusive transport of reacting species to or from the triple line [7]. In the first case, with control by local reaction kinetics, the rate of reaction and hence, the triple line velocity are expected to be constant with time [7]. This is approximately confirmed by experiment. Nearly constant triple line velocities $U = \mathrm{d}R/\mathrm{d}t$ (R being the drop base radius) have indeed been observed in the CuSi/C system [15,16] (see Fig. 1(a)), and also for unalloyed aluminium on carbon (for which diffusion clearly does not intervene) [7].

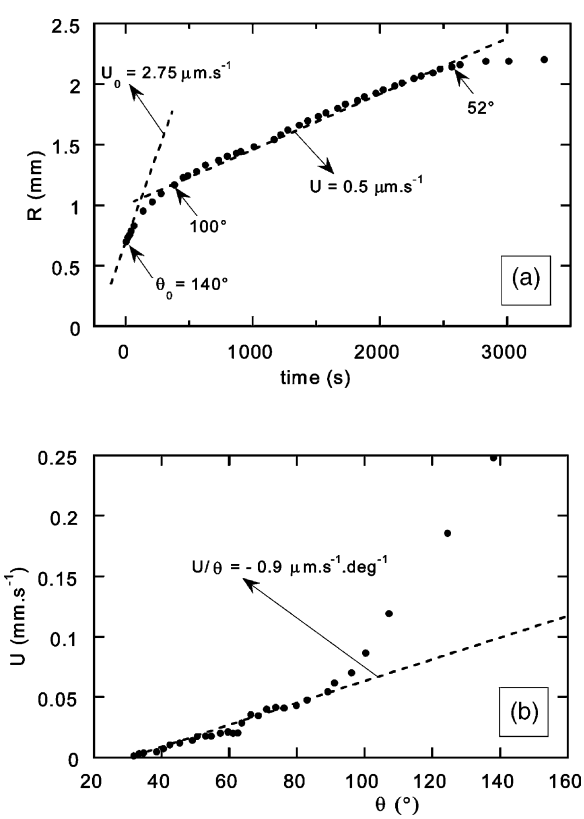

Fig. 1. Experimental curves of drop base radius versus time (a) Cu–40 at% Si alloy and of spreading rate U versus contact angle θ (b) Cu–1.5 at% Cr alloy on vitreous carbon substrates at 1150 °C [19].

In the second limit, diffusion is rate-limiting; local reaction rates are comparatively rapid, and the extent of local reaction which drives spreading is limited by the diffusive supply of reactant from the drop bulk to the triple line. According to Mortensen's model [8], the rate of isothermal spreading is time-dependent and varies in direct proportion to angle θ. This linear dependence has been verified in the Cu–Cr/C_v [17] (see Fig. 1(b)) and Cu–Sn–Ti/C_v [18] systems.

However, in both reaction-limited and diffusion-limited spreading, a considerable rise in triple line velocity U is observed in the high contact angle range (typically for $\theta > 100°$, see Fig. 1(a) and (b)). For instance, in both systems, at contact angles close to 140°, the triple line velocity exceeds by a factor of 3–5 the value expected by extrapolation to $\theta = 140°$ on the curves obtained at the low contact angle–long time range. The reasons for these deviations from the expected laws are not well established: in the case of 'reaction-limited' spreading it was suggested that this deviation is due to a transient configuration of the liquid/solid interface in the vicinity of the triple line which is not totally recovered by the reaction product [7]. Another possibility proposed by Voïtovich et al. [17] in the case of 'diffusion-limited' spreading, but also possible in the case of reaction-limited spreading, is reaction in front of the triple line occurring by evaporation–condensation of reactive solute. According to these authors, for geometrical reasons, such a mechanism would be active only for obtuse contact angles.

The aim of this study is to examine and quantify the influence of an evaporation–condensation process on reactive spreading kinetics in the sessile drop configuration. For this purpose a method is developed to express the quantity (given in number of monolayers) n of reaction product formed on the substrate surface in front of the triple line as a product of two terms: the quantity n_0 resulting from a simple ballistic exchange of reactive atoms in vacuum and a sticking coefficient β which is used to take into account kinetic limitations in the condensation of species on the substrate materials. For

a given system, the coefficient β is evaluated experimentally from Auger spectroscopic analysis using a simple configuration (that of the 'pendant drop'). The quantity n_0 is obtained by numerical calculations. This methodology is applied to two systems of reactive wetting. The first, Cu–Si/C is representative of reaction-limited spreading while the second, Cu–Cr/C is representative of diffusion-limited spreading.

2. Calculation of growth rate in front of the triple line

2.1. Expression of growth rate of a reaction product in front of the triple line

Consider a drop of metal B containing a solute A, on a carbon substrate under high vacuum. It is assumed that atoms A emitted from the drop surface to the substrate surface in front of the solid–liquid–vapour triple line can react with carbon and form the carbide A_xC_y according to the reaction:

$$[A] + \langle C\rangle \longrightarrow \langle A_xC_y\rangle \quad (1)$$

The flux, under vacuum, of a solute A from an elementary vapourising surface dS_1 of the drop with the normal $\vec{n}_1$ at its centre M to an elementary surface dS_2 of substrate C with the normal $\vec{n}_2$ at its centre N (Fig. 2) is given by [20]:

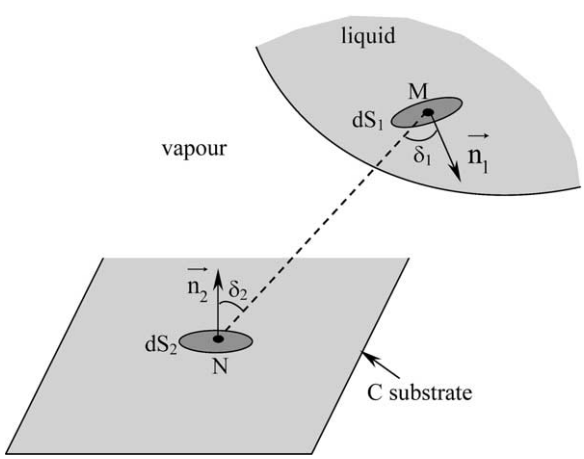

Fig. 2. Disposing of basic units of surface for the calculation of the flux of a component from an elementary vaporising surface dS_1 of the drop to an elementary surface dS_2 of a carbon substrate (see (2)).

$$d\Phi_A = \left(\frac{dN_A}{dS_2}\right) dS_1 \quad (2)$$

$$= \beta_e^L \frac{P^{sat}}{(2\pi M_A R_g T)^{1/2}\pi} \frac{(\overrightarrow{MN}\cdot\vec{n}_1)(\overrightarrow{MN}\cdot\vec{n}_2)}{(\overrightarrow{MN}\cdot\overrightarrow{MN})^2} dS_1 \ (\mathrm{molm^{-2}s^{-1}})$$

where dN_A is the number of evaporating moles of A from dS_1 and reaching dS_2 per unit time, M_A the molar mass of A, P^{sat} the partial pressure of A in equilibrium with the liquid drop at temperature T and R_g is the gas constant. The term $\beta_e^L(P^{sat}/(2\pi M_A R_g T)^{1/2})$ corresponds to the total evaporation flux of A from S_1 given by the Knudsen relation, $\beta_e^L(\leq 1)$ is an evaporation coefficient taking into account kinetics factors that may intervene during evaporation of A [21]. In general β_e^L is close to unity for liquid metals [21].

The integration of Eq. (2) along the part of the vaporising surface S_1 which can emit A atoms towards dS_2, noted S_1^*, leads to the total incident flux Φ^{inc} of A from S_1 to dS_2:

$$\Phi^{inc} = \int\int_{S_1^*} \left(\frac{dN_A}{dS_2}\right) dS_1 \quad (3)$$

$$= \frac{\lambda\, P^{sat}}{(2\pi M_A R_g T)^{1/2}} \ (\mathrm{molm^{-2}s^{-1}})$$

where λ is a geometric factor given by:

$$\lambda = \frac{1}{\pi}\int\int_{S_1^*} \frac{(\overrightarrow{MN}\cdot\vec{n}_1)(\overrightarrow{MN}\cdot\vec{n}_2)}{(\overrightarrow{MN}\cdot\overrightarrow{MN})^2} dS_1 \quad (4)$$

The elementary solid surface dS_2 emits itself a flux—reflected flux—Φ^{ref}, defined as the part of incident flux Φ^{inc} which does not participate in the growth of the reaction product. Φ^{ref} can be defined by introducing a condensation coefficient of A, β_c:

$$\beta_c = \frac{\Phi^{inc} - \Phi^{ref}}{\Phi^{inc}} \quad (5)$$

According to this definition the part of incident flux participating in the reaction product growth is $\beta_c\Phi^{inc}$. This is schematically shown in Fig. 3, where it is assumed that the carbon substrate is covered by isolated particles of the reaction product. The effective growth flux Φ^{gr} is equal to

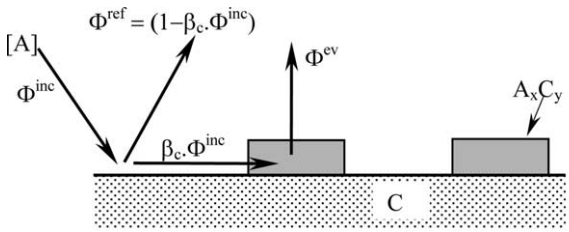

Fig. 3. Schematic configuration of the system: vaporising component [A]/C substrate/reaction product A_xC_y. Only the part $\beta_c\Phi^{inc}$ is captured by the growing reaction product. The net growth flux Φ^{gr} is equal to $\beta_c\Phi^{inc}$ minus the evaporation flux of A from the reaction compound.

$\beta_c\Phi^{inc}$ minus a flux Φ^{ev} which is the evaporation flux of A_xC_y:

$$\Phi^{gr} = \beta_c(^{inc}-^{ev}) \tag{6}$$

Φ^{ev} is linked with the partial pressure of A component in equilibrium with C and A_xC_y, P^{eq} , by the Knudsen equation:

$$\Phi^{ev} = \alpha\beta_e \frac{P^{eq}}{(2\pi M_A R_g T)^{1/2}} \tag{7}$$

(mole of A per m^2 of A_xC_y s^{-1}) where α is the surface coverage of C by A_xC_y and β_e is the evaporation coefficient of A from A_xC_y.

Combining Eqs. (3), (6) and (7) and assuming that, as for SiC/Si_{gaz} at high temperatures condensation and evaporation coefficients are equal, $\beta_c = \beta_e = \beta$ [22], the following expression of growth flux is obtained:

$$\Phi^{gr} = \frac{\beta}{(2\pi M_A R_g T)^{1/2}}[\lambda P^{sat} - \alpha P^{eq}] \tag{8a}$$

In the following (8a) will be used taking $\alpha = 1$:

$$\Phi^{gr} = \frac{\beta}{(2\pi M_A R_g T)^{1/2}}[\lambda P^{sat} - P^{eq}] \tag{8b}$$

The effect of this assumption on the calculated growth rate in systems with $\alpha < 1$ will be discussed subsequently. The value $\alpha = 1$ corresponds to a continuous layer of reaction product on the substrate. In this case, (8b) is still valid if the reaction layer is thin enough for diffusion of carbon atoms through this layer not to be limiting. Therefore, the thermodynamic activity of carbon on the free surface of reaction layer remains close to unity, as in the configuration of Fig. 3.

(8b) contains two terms, the driving force of condensation $[\lambda P^{sat} - P^{eq}]$ and the kinetic factor β. The growth of the reaction product A_xC_y may occur only if the driving force is positive, i.e. if $\lambda P^{sat} > P^{eq}$. This driving force depends on the thermodynamic quantities P^{sat} and P^{eq} which are constant for a given alloy/substrate system at fixed temperature, and on the geometrical factor λ depending only on the geometrical configuration of the system (see (4)). This factor λ is now calculated for the sessile drop configuration and a static triple line.

2.2. Calculation of geometrical factor λ in the case of a static triple line

Numerical calculations of factor λ have been performed for an elementary surface around a given point N of substrate. This point is located at a distance L from an immobile triple line of a drop defined by its drop radius r and contact angle θ (Fig. 4). The integration area S_1^* for (4) is defined by two angular coordinates φ and ϵ (Fig. 4). φ varies from $\varphi*$ to θ, with $\varphi*$ verifying the equation:

$$L\sin\varphi^* + r\cos\theta\cos\varphi^* = r \tag{9}$$

whereas for a given value of φ, ϵ varies between $-\epsilon*$ and $\epsilon*$, with:

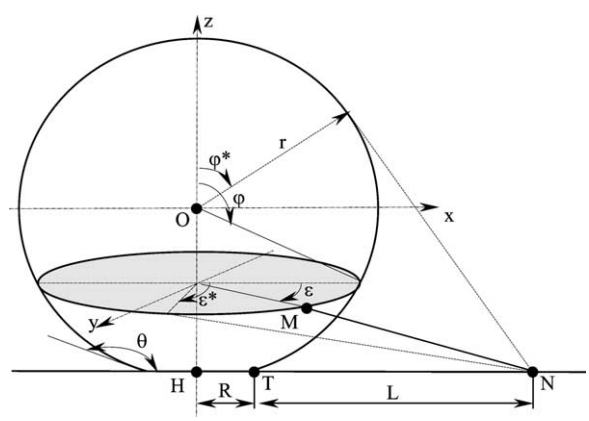

Fig. 4. Schematic configuration of the drop/substrate system showing the arrangement of basic units (see Eqs. (9) and (10)) for numerical calculation of geometrical factor λ (4)).

$$\varepsilon^* = \arccos\left[\frac{r\,(1-\cos\varphi\cos\theta)}{L\sin\varphi}\right] \qquad (10)$$

The angular coordinates ϵ and φ were discretised using 1000 grids in both directions since a doubling of the resolution was found to change the numerical results by less than 0.1%.

For the two particular cases $\theta = 90$ and 180°, analytical expressions of the geometrical factor λ have been found (see Appendix). Fig. 5 shows the λ versus the distance L from the triple line curves, obtained from the analytical and numerical calculations for a drop radius of 1 mm and two contact angles 90 and 180°. The difference between analytical and numerical values of λ is less than 0.5% which confirms the validity of numerical calculations.

It is important to note that, thanks to the oz-axial symmetry of the model, for any contact angle θ, the geometrical factor λ depends only on the ratio L/r, regardless of the r and L values. This statement is verified from the analytical expression of λ for $\theta = 90$ and 180° (Eqs. (A12) and (A14)). This is also confirmed from numerical results obtained for other contact angle values, as indicated in Fig. 6(a) which shows the variation of λ as a function of L/r for different contact angle values and for two drops of radius 1 and 2 mm, respectively. Moreover, it is seen that when L/r tends to zero, i.e. when N tends to the triple line (see Fig. 4), $\lambda(\theta, L/r)$ tends to a limit value $\lambda_0(\theta)$. This value is almost reached

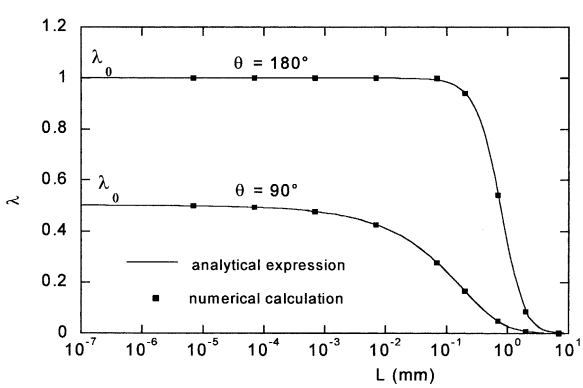

Fig. 5. The geometrical factor λ versus the distance from the triple line L, obtained from analytical (—) and numerical (■) calculations for a drop radius of 1 mm and two contact angles: $\theta = 90$ and 180°.

for $L/r < 10^{-2}$ i.e. for $L < 10^{-2}$mm in the case of a droplet with $r = 1$mm. Note that the values of λ become significant ($\lambda/\lambda_0 > 1\%$) only for $L/r < 3$, i.e. for $L < 3$mm in the case of a droplet with $r = 1$mm.

In Fig. 6(b) λ_0 is given as a function of the contact angle θ. As expected intuitively λ_0 vanishes for $\theta = 0°$ and is equal to unity for $\theta = 180°$. The variation of λ_0 between these two values is relatively smooth.

3. Application to cu–40 at% si and cu–1.5 at% cr alloys on C_v substrate

In this paragraph the growth rate of the reaction product in front of the triple line is calculated in the particular case of $\beta = 1$ corresponding to the maximum growth rate value $^{gr}_{max}$. Moreover, it is assumed that the reaction product forms a thin continuous layer, i.e. $\alpha = 1$. Calculations are first performed for an immobile triple line and a fixed value of contact angle. Then further calculations will be done for a triple line moving from θ_0 to θ_F.

3.1. Static triple line

The above calculations are applied to the Cu–40 at% Si and Cu–1.5 at% Cr drops on a carbon substrate at 1150 °C. The maximum growth flux of the reaction product, calculated from Eq. (8b) with $\beta = 1$, can be expressed in terms of the number of monolayers per unit time knowing the molar area $\Omega_{A_xC_y}$ of the reaction product A_xC_y (A=Si or Cr):

$$v^{gr}_{max} = \frac{\Omega_{A_xC_y}}{x}\frac{1}{(2\pi M_A R_g T)^{1/2}}[\lambda P^{sat} - P^{eq}] \ (A_xC_y \text{ monolayers s}^{-1}) \qquad (11)$$

The values of P^{sat} and P^{eq} calculated from thermodynamic data at 1150 °C [23] as well as the values of the molar areas calculated from molar volumes V_m using the classical relation $\Omega_{A_xC_y} \approx [(x + y)N_{Av}]^{1/3}V_m^{1/3}$ (N_{Av}=Avogadro's number) are reported in Table 1. (The values of V_m are from Refs. [24] and [25].)

Fig. 7 presents the variation in the maximum growth rate of SiC and Cr_7C_3 carbides on the car-

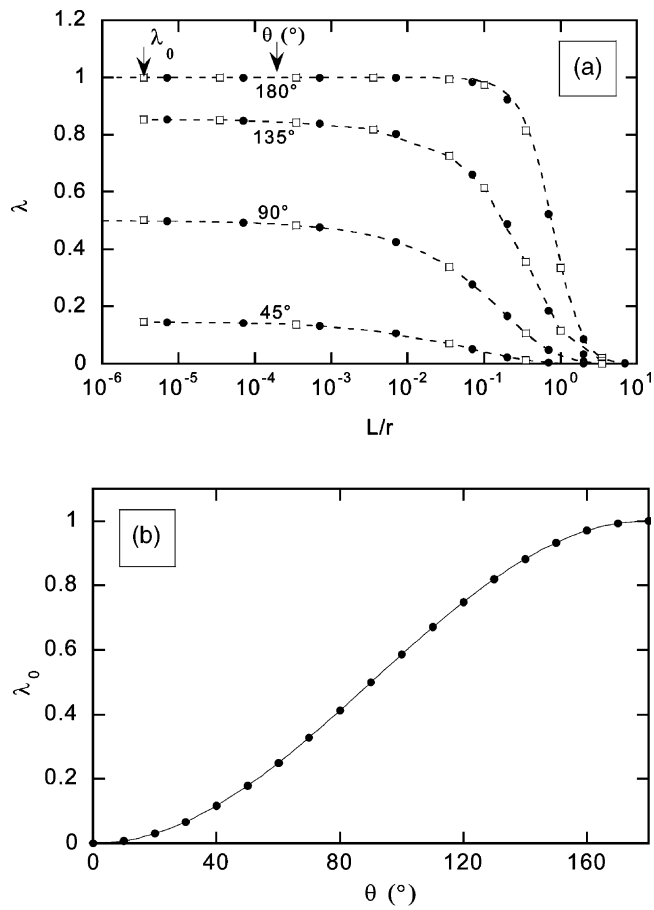

Fig. 6. (a) Variation of geometrical factor λ as a function of the ratio of the distance from the triple line L to the drop radius r for two drops of radius 1 mm (●) and 2 mm (□), respectively. (b) Variation of the limit value (λ_0) of the geometrical factor λ when L/r tends to zero with the contact angle θ (r = 1mm).

bon substrate in front of the triple line for a droplet of radius 1 mm and $\theta = 120°$. It is shown that the maximum growth rate of Cr_7C_3 is significant even at a distance of 0.7 mm in front of the triple line whereas its values for SiC are more than one order of magnitude lower (even at the triple line, where the growth rate takes its highest value, this rate is only 0.15 monolayers.s^{-1}).

In Section 3.2 the number of the reaction product layers formed in front of the triple line will be calculated for a triple line moving from θ_0 to θ_F.

3.2. Moving triple line

The aim is to find out whether the excess spreading rates observed for Cu–Si and Cu–Cr alloys in the high contact angle range with respect to the spreading rates found in the low θ range (Fig. 1) are due to reaction product growth occurring in front of the triple line by an evaporation–condensation mechanism.

For this purpose, the number of reaction product monolayers formed during spreading ahead of the triple line is calculated assuming that spreading in the high θ range occurs according to the laws observed for low θ. Thus, in the case of the Cu–Si/C_v couple, a unique value $U = 0.5\mu ms^{-1}$ is used for the entire process for $40 < \theta < 140°$ and, for the Cu–Cr/C_v couple, spreading will be described by the same value $U/\theta = -0.9 mms^{-1}deg^{-1}$ for $30 < \theta < 155°$.

Any significant increase in the calculated num-

Table 1
Equilibrium Si and Cr pressure corresponding respectively to Cu–40 at% Si and Cu–1.5 at% Cr alloys at 1150 °C and molar areas Ω of SiC and Cr_7C_3

	P^{sat} (Pa)	P^{eq} (Pa)	Ω_{SiC} (m^2 mol^{-1})	$\Omega_{Cr_7C_3}$ (m^2 mol^{-1})
Cu–40 at% Si	1.25×10^{-4}	9.52×10^{-7}	5.73×10^{4}	
Cu–1.5 at% Cr	9.45×10^{-3}	8.88×10^{-4}		27.2×10^{4}

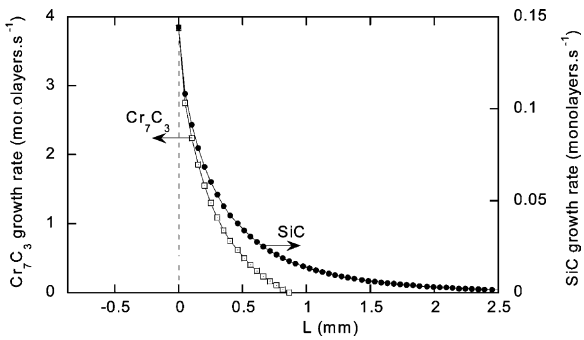

Fig. 7. Variation of the maximum growth rate of SiC and Cr_7C_3 at 1150 °C on different points of the carbon substrate as a function of their distance L from the triple line for an immobile triple line and a contact angle $\theta = 120°$ (drop radius is $r = 1$mm and the centre of drop base is at $L \approx -0.87$mm).

ber of carbide monolayers accumulated ahead of the moving triple line found in the high θ range compared to the range of low θ values will be considered as giving evidence of the role of evaporation–condensation on spreading kinetics.

Numerical calculations are performed as follows: during the spreading of the drop from θ_0 to θ_F, for any point N (Fig. 8) of the substrate located before spreading at a distance L from the triple line, the number of monolayers of the reaction product growing during the time needed for the triple line to move from N_0 to N is computed. The calculations are carried out in steps of 10 μm, a value which is two orders of magnitude lower than the total displacement of the triple line.

Fig. 9(a) and (b) shows the variation in the number of reaction product monolayers formed on the substrate at a distance of 10 μm from the triple line (where the value of λ is close to the plateau value λ_0, Fig. 6(a)), as a function of the instantaneous contact angle θ. It is seen that the number of

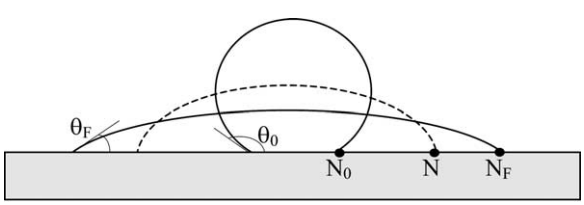

Fig. 8. Successive positions of the triple line during the spreading of a drop from the initial contact angle θ_0 to the final contact angle θ_F.

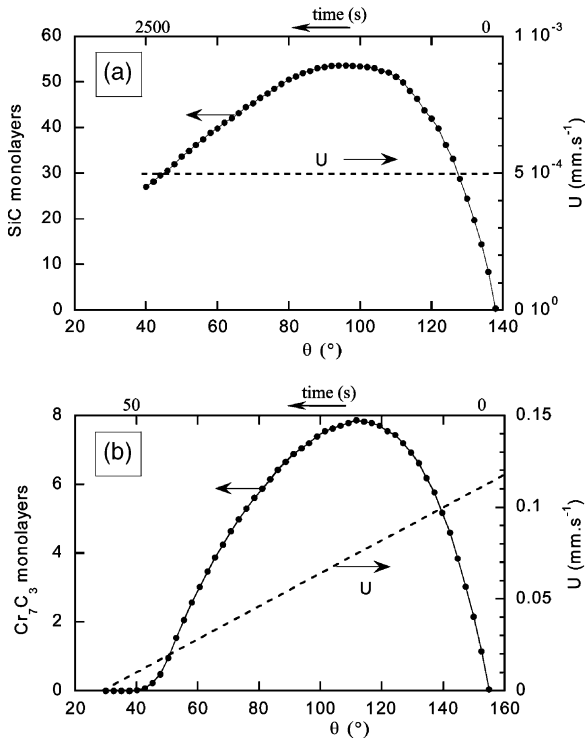

Fig. 9. Variation of the calculated number of the reaction product monolayers formed during spreading on the substrate at a distance of 10 μm in front of the triple line as a function of the instantaneous contact angle θ: (a) Cu–40 at% Si/C_v couple: constant triple line velocity $U = 0.5\mu ms^{-1}$, (b) Cu–1.5 at% Cr/C_v couple: $U/\theta = -0.9\mu ms^{-1}deg^{-1}$. Drop radius $r =$ 1mm, $T = 1150°C$.

accumulated reaction product monolayers is higher for SiC than for Cr_7C_3 by a factor of five at any θ value, despite the fact that SiC growth rate is about 30 times lower than Cr_7C_3 growth rate (see Fig. 7). This is because the spreading time for Cu–Si alloy, and as a result the time of ballistic exchanges between the C_v substrate and the drop, is much longer than for the Cu–Cr alloy (2500 s against 50 s).

From these results it cannot be excluded that the evaporation–condensation might influence the spreading rate; final conclusion on this point will be given once the value of $\beta = \Phi^{gr}_{exp}/\Phi^{gr}_{max}$ is known. However, given the shape of calculated curves, the assumption that the higher spreading rate at high θ values results from the evaporation–condensation mechanism can since now be

excluded. Indeed, while the triple line velocity remains constant (Fig. 9(a)) or increases with θ monotonically (Fig. 9(b)), the accumulated number of monolayers passes through a maximum and decreases rapidly at $\theta > 100°$ (Fig. 9(a)) and $\theta > 120°$ (Fig. 9(b)). Note that this maximum is due to the opposite effects of an increase of θ on the number of accumulated reaction product monolayers at fixed exchange time (this number increases with θ) and on the exchange time (this time decreases with θ).

3.3. Determination of the evaporation–condensation coefficient

The evaporation–condensation coefficient β for Cu–40 at% Si and Cu–1.5 at% Cr alloys is evaluated by combining the calculated maximum value of monolayers n_{rp}^{max} of the reaction product formed on the carbon substrate with the experimental value n_{rp}^{exp} obtained for the same configuration and time:

$$\beta = \frac{n_{rp}^{exp}}{n_{rp}^{max}} \tag{12}$$

The configuration used is that of the pendant drop (Fig. 10) for which a simple analytical expression of the geometrical factor λ is found corresponding

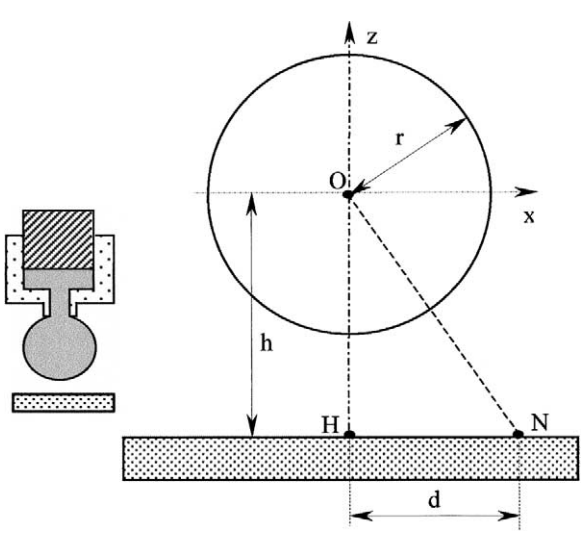

Fig. 10. Schematic presentation of the pendant drop configuration. The different symbols are explained in the text.

to any point N of the substrate situated at a distance d from the point H (see Fig. 10 (A15)):

$$\lambda = \frac{h\, r^2}{[d^2 + h^2]^{3/2}} \tag{13}$$

For r = 1mm and h = 1.17mm, the values of λ calculated from (13) vary from 0.73 to 0.57 when d varies between 0 and 0.5 mm, respectively.

Using (11) with data given in Table 1 and λ values varying from 0.57 to 0.73 and for t = 15min, the maximum values of calculated number of Cr_7C_3 and SiC monolayers are, $n_{Cr_7C_3}^{max}$ = 2500–3400 and n_{SiC}^{max} = 130–180, respectively.The experimental value of n_{rp} was evaluated by performing pendant drop experiments in a metallic furnace under a vacuum of 10^{-5} Pa at T = 1150°C, i.e. in conditions close to those used in the experiments of Fig. 1. The apparatus consists essentially of a molybdenum heater surrounded by molybdenum radiation shields, located in a water-cooled stainless-steel chamber. The drop images were produced using an optical system fitted with a zoom (magnification 30×). This device enables the drop radius and the distance between the drop and the substrate to be obtained with an accuracy of ± 2%.

The vitreous carbon substrates (V25 vitreous carbon, featuring no open porosity, an ash content less than 50 ppm and a density 1500–1550 kg m^{-3}, provided by Le Carbone-Lorraine, France) were mechanically polished to a 1 μm diamond paste. Measured height variations along the polished substrate surface were of amplitude between 1 and 2 nm and wavelength was between 10 and 20 μm.

The Cu–Si and Cu–Cr alloys used are prepared from pure Cu (99.999 wt%), Si (99.9995 wt%) and Cr (99.3 wt%) by melting and alloying in an alumina crucible (Fig. 10) during experiments performed in high vacuum (10^{-5} Pa). Once the experiment temperature of 1150 °C is attained, the liquid is extruded from the crucible (see Fig. 10) forming a drop which was maintained at a distance $h-r$ from the carbon substrate (with r = 1mm and h = 1.17mm) for 15 min.

After cooling, the area of carbon substrate located under the drop was characterised by Auger microprobe. Taking into account the dimension of the Auger spectroscopy probe used (1 μm), it is

difficult to ensure that the characterised area is located exactly at the point H (see Fig. 10). Nevertheless, the distance from this point is certainly lower than 0.5 mm.

In the case of Cu–1.5 at% Cr drop, the Auger analysis performed at many places on the carbon substrate surface around point H occasionally gives evidence of the presence of chromium as shown in Fig. 11. This weak chromium signal could not be due to a possible Cr condensation during cooling, not only because of the very low Cr pressure, but also because of the local nature of the detected Cr signal. Therefore, the Cr signal is attributed to the Cr exchange between the drop and carbon substrate during the pendant drop experiment. Nevertheless, the small peaks shown by arrows just beside the carbon peak are characteristics of carbide formation [26]. The very low quantity of Cr detected suggests the formation of Cr carbide as isolated particles at a very low surface coverage.

In order to highlight these particles, the carbon surface was analysed by high resolution optical profilometry in order to study relatively large areas (~10^4 μm^2). No particle mounds were found meaning that the particles, if any, would have a height close to or less than the vertical resolution of the profilometer (~1 nm).

In view of the very low value of $n^{\exp}_{Cr_7C_3}$, a quantitative evaluation of this parameter is not possible. A rough estimation of $n^{\exp}_{Cr_7C_3}$ is 10^{-2} with an uncertainty of one order of magnitude: ($n^{\exp}_{Cr_7C_3} = 10^{-2\pm1}$) [26].

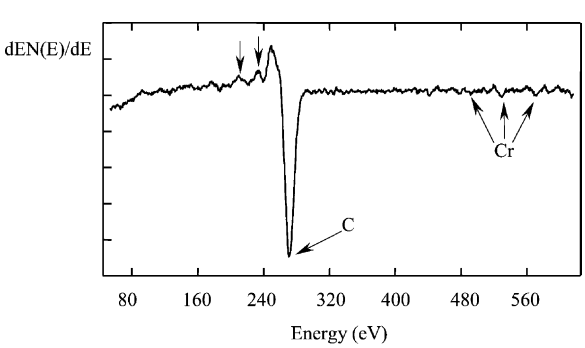

Fig. 11. Auger spectra of the surface of the C_v substrate obtained after the pendant drop experiment. The small peaks shown by arrows just beside the carbon peak indicate carbide formation.

From experimental and calculated values of Cr_7C_3 monolayers and (12), the value of the evaporation–condensation coefficient β in the Cu–Cr/C_v system is $\leq(10^{-2\pm1}/3\times10^3)\approx3\times10^{-6\pm1}$.

In the case of a Cu–40 at% Si drop, the Auger analysis did not detect any Si signal on the vitreous carbon substrate meaning that the possible quantity of SiC on this surface would be lower than the resolution of Auger spectroscopy, i.e. $n^{\exp}_{SiC} < 10^{-2}$, leading to $\beta_{Si} < (10^{-2}/2\times10^2) = 5\times10^{-5}$.

From the above values of β_{Cr} and β_{Si} the number of monolayers of SiC and Cr_7C_3 corresponding to the maximum of curves of Fig. 9(a) and (b) are: $n_{SiC} = \beta_{Si} n^{\max}_{SiC} < 3\times10^{-3}$ and similarly $n_{Cr_7C_3} = \beta_{Cr} n^{\max}_{Cr_7C_3} \leq 3\times10^{-5\pm1}$. These results clearly indicate that the evaporation–condensation process in front of the triple line cannot influence the Cu–Cr and Cu–Si spreading on vitreous carbon.

The calculation of $n^{\max}_{rp}$ was performed taking $\alpha = 1$ in (8a). Actually this value is lower (and even much lower) than one. It can be readily seen that using a value $\alpha < 1$ in (8a) yields a higher value of $n^{\max}_{rp}$ and a lower value of β ((12)). Hence, the above conclusion on the possible role of evaporation–condensation remains a fortiori valid and confirms the conclusion drawn in Section 3.2 from the shape of calculated $n^{\max}_{rp}$ versus θ curves: this phenomenon is not at the origin of the spreading acceleration on the high θ range observed for both systems (Fig. 1). Note that the reaction of metal atoms with the substrate material in front of the triple line can be produced not only by evaporation–condensation, but also by surface diffusion. However, surface diffusion does not depend on the contact angle θ and thus can hardly explain the acceleration of the triple line at high θ. The origin of this acceleration in the case of Cu–Si/C_v system is the object of another study [27].

The very low, and even negligible reactivity, between Cr or Si atoms emitted by the Cu-base alloys and vitreous carbon surface at 1150 °C in high vacuum may appear surprising. This result indicates that the interactions developed between the incident Si or Cr atoms and C atoms of the substrate are very weak except probably at a limited number of sites. This behaviour, which is typi-

cal of graphitic surfaces, is related with the microstructure of vitreous carbon, which is also graphitic although imperfectly crystallised form of carbon. A consequence of this microstructure is that, the initial average interactions between molten silicides and vitreous carbon, as quantified by contact angle measurements [27], are van der Waals interactions. However, with other ceramics, as oxides or certain nitrides, the initial interactions between reactive alloys and ceramic surfaces may be strong. In this case a significant role of evaporation–condensation on spreading kinetics may be expected.

4. Conclusion

A general method is described to study the effect on spreading of a reaction occurring in front of an advancing triple line, by evaporation–condensation in high vacuum.

For this purpose, a method is developed to evaluate the thickness of the reaction product in front of the triple line during spreading. In this method, a calculation of ballistic exchange between the drop surface and the substrate surface is coupled to Auger spectroscopic analysis of the substrate surface.

The method is applied to the case of Cu–Cr and Cu–Si liquid droplets on vitreous carbon substrate, chosen as representative of two major types of reactive spreading (diffusion-limited and reaction-limited, respectively). It is shown that the acceleration of spreading observed for both systems at high contact angles is not due to an evaporation–condensation process.

As will be shown in Ref. [26], this acceleration results from the reaction process at the molten drop/substrate interface behind the triple line.

Acknowledgements

This work was in part supported by NEDO International Research Grant (project 'Wettability of Solids by Liquids at High Temperature') supervised by the Ministry of Economy, Trade and Industry of Japan. Also the authors acknowledge Christian Chatillon (LTPCM) for helpful discussions relating to condensation–evaporation phenomena.

Appendix

Analytical expression of the geometric factor λ in the case of a sessile drop configuration for particular values of contact angle $\theta = 0{,}90$ and 180° and in the case of a pendant drop configuration.

Sessile drop configuration

The drop/substrate system is shown in Fig. A1. For a given drop radius r and contact angle θ, the expression of λ corresponding to a point N of the substrate is given by (3):

$$\lambda = \frac{1}{\pi}\int\int_{S_1^*} \frac{(\overrightarrow{MN}\cdot\vec{n}_1)(\overrightarrow{MN}\cdot\vec{n}_2)}{(\overrightarrow{MN}\cdot\overrightarrow{MN})^2} dS_1 \qquad \text{(A1)}$$

In (A1) dS_1 is an elementary vaporising surface with the outward unit normal $\vec{n}_1$ at its centre M, $\vec{n}_2$ the normal to substrate at N and S_1^* is the visible part of the drop from N.

The surface drop is described as a spherical cap in a 3-dimensional space by the equation:

$$x^2 + y^2 + z^2 = r^2 \qquad \text{(A2)}$$

In Fig. A1, the point H represents the orthogonal projection of the drop centre O(0,0,0) on the substrate plane P which is taken parallel to the y axis. Moreover, the distances ON and OH are noted by a and h, respectively. The coordinates of points M, N and H are then as follows:

$$M(x,y,z)\ N(a,0,0)\ H\left(\frac{h^2}{a},\ 0,\ \pm\frac{h}{a}(a^2-h^2)^{1/2}\right)$$

The coordinates of $\overrightarrow{MN}$ and of normals $\vec{n}_1$ (parallel to OM) and $\vec{n}_2$ (parallel to OH) can then be easily calculated:

$$\overrightarrow{MN} = (x-a,y,z)\ \vec{n}_1 = \frac{1}{r}(x,y,z)\ \vec{n}_2 \qquad \text{(A3)}$$

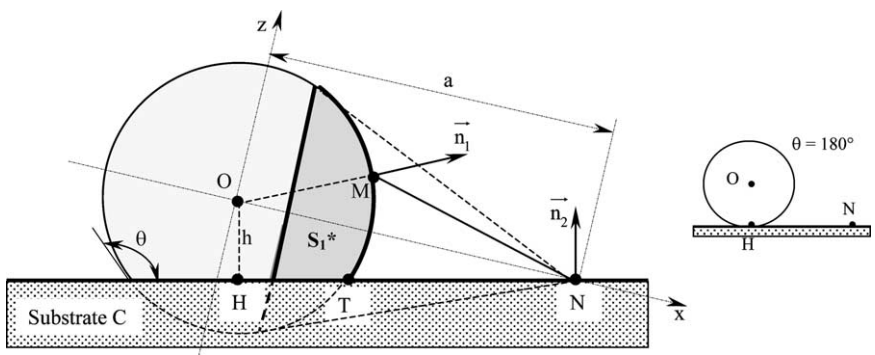

Fig. A1 Schematic presentation of a sessile drop configuration showing the arrangement of *x,y,z* axis and basic units used for analytical calculations of the geometrical factor λ.

$$= \left(\pm \frac{h}{a},\ 0,\ \frac{(a^2-h^2)^{1/2}}{a} \right)$$

with, for $\vec{n}_2$, the sign '+' if the centre of the drop is situated under the substrate plane P($z_H < 0$) and '−' otherwise ($z_H > 0$).

$D*$ is the projection of S_1^* on the y–z plane. S_1^* is then defined by a continuous function on $D*$: $x = (r^2-y^2-z^2)^{1/2}$. Then, for a given elementary surface $dS_{D*} = dydz$ on the domain $D*$, the corresponding elementary surface dS_1 on S_1^* can be easily calculated:

$$dS_1 = \frac{r}{(r^2-y^2-z^2)^{1/2}} dydz \qquad \text{(A4)}$$

Substituting in (A1) $\overrightarrow{MN}$, $\vec{n}_1$, $\vec{n}_2$ and dS_1 given by Eqs. (A3) and (A4), and integrating over the domain D$*$ the expression of λ is obtained:

$$\lambda(a,h) \qquad \text{(A5)}$$

$$= \frac{1}{a\pi} \iint_{D^*} \frac{(a(r^2-y^2-z^2)^{1/2}-r^2)(\pm h(r^2-y^2-z^2)^{1/2}-a) + z(a^2-h^2)^{1/2})}{(r^2 + a^2-2a\sqrt{r^2-y^2-z^2})^2(r^2-y^2-z^2)^{1/2}} dydz$$

For fixed values of a and r this integral is calculated in the particular cases:

$h = +r(\theta = 0°)$, $h = 0(\theta = 90°)$ and $h = -r(\theta = 180°)$.

Case 1:
$h = +r$, i.e. $z_H = +r(\theta = 0°)$.

In this case the plane P is tangent to the sphere and the visible part of the sphere from N is reduced to the point M. Both normals $\vec{n}_1$ and $\vec{n}_2$ are orthogonal to $\overrightarrow{MN}$ which gives $\overrightarrow{MN}\cdot\vec{n}_1 = \overrightarrow{MN}\cdot\vec{n}_2 = 0$, and thus from (A1) $\lambda = 0$ is obtained.

Case 2:
$h = 0(\theta = 90°)$.

(A5) for $h = 0$ becomes:

$$\lambda(a,0) \qquad \text{(A6)}$$

$$= \frac{1}{\pi} \iint_{D^*} \frac{z(a(r^2-y^2-z^2)^{1/2}-r^2)}{(r^2 + a^2-2a\sqrt{r^2-y^2-z^2})^2(r^2-y^2-z^2)^{1/2}} dydz$$

In this case, the integration domain $D*$ consists in the half-circle $y^2 + z^2 \le r_D^2$, $z \ge 0$ - with $r_D = \frac{r}{a}(a^2-r^2)^{1/2}$. (A6) is integrated introducing polar coordinates:

$$y = \rho\cos\theta,\ z = \rho\sin\theta \text{ and the Jacobian } J = \rho \qquad \text{(A7)}$$

The transformed integration domain in polar coordinates is then given by:

$$0 \le \rho \le r_D,\ 0 \le \theta \le \pi \qquad \text{(A8)}$$

Under these conditions (A6) is transformed into:

$$\lambda(a,0) \qquad \text{(A9)}$$

$$= \frac{1}{\pi} \int_0^{\pi} \sin\theta d\theta \int_0^{r_D} \frac{\rho^2(a(r^2-\rho^2)^{1/2}-r^2)}{(r^2 + a^2-2a\sqrt{r^2-\rho^2})^2(r^2-\rho^2)^{1/2}} d\rho$$

After integrating (A9) by parts the following expression is obtained:

$$\lambda(a,0) = \frac{1}{\pi}\Bigg[-\frac{r}{a^2}(a^2-r^2)^{1/2} + \frac{a^2+r^2}{2a^2}\arctan\left(\frac{a+r}{a-r}\right)^{1/2} - \frac{a^2-r^2}{4a^2}\arcsin\left(\frac{(a^2-r^2)^{1/2}}{a}\right) + \frac{1}{2}\arcsin\left(\frac{r}{a}\right) - \frac{\pi r^2}{4a^2}\Bigg] \quad \text{(A10)}$$

For $\theta = 90°$, $a = r + L$ where L is the distance of N from the triple line T. If:

$$b = \frac{r}{a} = \left[1 + \frac{L}{r}\right]^{-1} \quad \text{(A11)}$$

then (A10) becomes:

$$\lambda(b) = \frac{1}{\pi}\Bigg[-b(1-b^2)^{1/2} + \frac{1+b^2}{2}\arctan\left(\frac{1+b}{1-b}\right)^{1/2} - \frac{1-b^2}{4}\arcsin(1 - b^2)^{1/2} + \frac{1}{2}\arcsin(b) - \frac{\pi b^2}{4}\Bigg] \quad \text{(A12)}$$

The above equation shows that λ depends only on the ratio $L/r(=b)$. Moreover, it is easily verified from this equation that λ corresponding to a point N of the substrate tends to 0.5 when the distance L of this point from the triple line T, tends to 0^+.

Case 3:
$h = -r$, i.e. $z_H = -r(\theta = 180°)$.

In this case $a = L$, the integration domain $D*$ consists of the whole circle $y^2 + z^2 \leq r_D^2$ with $r_D = (r/a)(a^2-r^2)^{1/2}$ and the transformed integration domain in polar coordinates is given by:

$$0 \leq \rho \leq r_D,\ 0 \leq \theta \leq 2\pi \quad \text{(A13)}$$

The same calculations as above give:

$$\lambda = \frac{r^3}{(r^2+L^2)^{3/2}} = \left[1 + \left(\frac{L}{r}\right)^2\right]^{3/2} \quad \text{(A14)}$$

(A13) shows that λ depends only on the ratio (L/r) and that λ tends to 1 when the distance L of the point N from the triple line T, tends to 0^+.

Dispensed drop ($h > r$, i.e. $z_H > r$).

When $h > r$ (see Fig. 10), the same calculations as in the case of the sessile drop configuration for $h = +r(\theta = 180°)$ with $a = (d^2 + h^2)^{1/2}$ are performed.The following expression of λ is then obtained:

$$\lambda = \frac{hr^2}{(h^2+d^2)^{3/2}} \quad \text{(A15)}$$

Finally, note that in this case λ depends only on the ratios (h/r) and (d/r):

$$\lambda = \frac{h}{r}\left[\left(\frac{h}{r}\right)^2 + \left(\frac{d}{r}\right)^2\right]^{-3/2} \quad \text{(A16)}$$

References

[1] Naidich Y. In: Cadenhead DA, Danielli JF, editors. Progress in surface and membrane science. New York: Academic Press; 1981. p. 353.
[2] Nogi K. Trans JWRI 1993;22:183.
[3] Eustathopoulos N, Nicholas N, Drevet B. Wettability at high temperatures. In: Pergamon materials series. Amsterdam: Elsevier; 1999. p. 115.
[4] Eustathopoulos N, Drevet B. J Phys 1994;III 4:1865.
[5] Landry K, Rado C, Voitovich R, Eustathopoulos N. Acta mater 1997;45:3079.
[6] Ambrose JC, Nicholas MG, Stoneham AM. Acta Metall Mater 1993;41:2395.
[7] Landry K, Eustathopoulos N. Acta mater 1996;44:3923.
[8] Mortensen A, Drevet B, Eustathopoulos N. Scr Mater 1997;36:645.
[9] Meier A, Chidambaram PR, Edwards GR. Acta mater 1998;46:4453.
[10] Saiz E, Cannon R, Tomsia A. Acta mater 1998;48:4449.
[11] Yost F, O'Toole E. Acta mater 1998;46:5143.
[12] Warren J, Boettinger W, Roosen A. Acta mater 1998;46:3247.
[13] Nomura M, Iwamota C, Tanaka S. Acta mater 1999;47:407.
[14] Ebrill N, Durandet Y, Strezov L. Trans JWRI 2001;30:251.
[15] Landry K, Rado C, Eustathopoulos N. Metall Trans A 1996;27A:3181.
[16] Dezellus O, Hodaj F, Eustathopoulos N. In: Eustathopoulos N, Sobczak N, editors. Proceedings of the International Conference on High Temperature Capillarity, Cracow, Poland, 1997. 1998. p. 18.
[17] Voitovitch R, Mortensen A, Hodaj F, Eustathopoulos N. Acta mater 1999;47:1117.
[18] Dezellus O, Hodaj F, Mortensen A, Eustathopoulos N. Scr Mater 2001;44:2543.

[19] Dezellus O. Thesis, Institut National Polytechnique de Grenoble, France; 2000.
[20] Vassent JL, Marty A, Gilles B, Chatillon C. Vacuum 2002;64:65.
[21] Pound GM. J Chem Ref Data 1972;1:135.
[22] Chatillon C, Rocabois P, Bernard C. High Temp–High Pressures 1999;31:413.
[23] Chase MW. NIST-JANAF Thermochemical Tables, Monograph No 9. Published by the American Chemical Society and the American Institute of Physics for the National Institute of Standards and Technology; 1998.
[24] Brandes EA, Brook GB, editors. Smithells metals reference book. 7th ed. Butterworth and Heinemann; 1992. p. 272.
[25] Masson et Cie editors. Nouveau traité de chimie minerale, tome XII. Paris 1959. p. 367.
[25] Joud JC. LTPCM-ENSEEG, Institut National Polytechnique de Grenoble, personal communication.
[26] Dezellus O, Hodaj F, Eustathopoulos N. Acta mater, this issue.